

Cooperative effect of electronic and nuclear stopping on ion irradiation damage in silica

M Backman^{1,2}, F Djurabekova², O H Pakarinen², K Nordlund²,
Y Zhang^{3,1}, M Toulemonde⁴ and W J Weber^{1,3}

¹ Department of Materials Science and Engineering, University of Tennessee,
Knoxville, Tennessee 37996, USA

² Helsinki Institute of Physics and Department of Physics, P.O. Box 43, FI-00014
University of Helsinki, Finland

³ Materials Science and Technology Division, Oak Ridge National Laboratory, Oak
Ridge, Tennessee 37831, USA

⁴ CIMAP-CEA-CNRS-ENSICAEN-University of Caen, F-14070 Caen Cedex 5,
France

E-mail: marie.backman@gmail.com

Abstract. Radiation damage by ions is conventionally believed to be produced either by displacement cascades or electronic energy deposition acting separately. However, there is a range of ion energies where both processes are significant and could contribute to irradiation damage. The combination of two computational methods, namely binary collision approximation and molecular dynamics, the latter with input from the inelastic thermal spike model, makes it possible to examine the simultaneous contribution of both mechanisms of energy deposition on the structural damage in the irradiated structure. We study the effect in amorphous SiO₂ irradiated by Au ions with energies ranging between 0.6 and 76.5 MeV. We find that in the intermediate energy regime, there is a synergistic effect of local heating due to electronic excitations in enhancing the displacement cascade damage.

PACS numbers: 61.80.Jh, 61.43.Bn, 61.43.Fs

1. Introduction

Ion irradiation of solids is a topic that is studied both as a tool for materials modification and as a source of damage to materials in, for instance, nuclear reactors. Conventionally, ion irradiation damage is thought to be due to either nuclear or electronic energy loss acting separately [1]. Moreover, damage from electronic processes is believed to be produced only above a threshold in electronic stopping power [2, 3, 4]. However, in the energy regime just above the ion track threshold, nuclear damage is still significant and one can thus pose the question whether the two damage formation mechanisms might act at the same time.

Amorphous SiO_2 is one component of borosilicate glasses used for immobilization of radioactive waste from nuclear reactors [5]. Silica glasses are also common in many microelectronic devices, which may be exposed to particle irradiation both under fabrication and in operation. Due to its applications in high radiation environments, the literature on the response of silica to irradiation damage from both displacement and ionization processes is extensive, however, little is yet known about how the interplay between displacement and ionization processes affects observed irradiation damage.

Structural damage due to electronic excitation processes during ion irradiation of silica has been discussed in, for example, [5, 6, 7, 8, 9, 10, 11, 12]. Presby and Brown [6] measured damage from electronic and nuclear stopping and estimated the latter mechanism to be about 200 times more effective in creating a change in refractive index. EerNisse and Norris [7] showed that damage from collision cascades and electronic excitations are annealed at different temperatures and found indications of a dose rate dependent interaction between the two damage mechanisms.

To date, only a few studies have been published on the interplay between nuclear and electronic stopping on irradiation damage processes in silica. Jaque and Townsend varied ion species and energies, thereby varying relative magnitudes of electronic and nuclear stopping powers, and measured luminescence spectra from irradiated SiO_2 [8]. Their results indicated that ionization processes are involved in damage formation under irradiation. In a similar setup, Toulemonde *et al* irradiated silica with Au ions of varying energy and found evidence for a synergy effect in the intermediate energy range [13]. Contrary to these observations, Nagata *et al* [14] found competing damage formation and annihilation by nuclear and electronic stopping, respectively, for H and He ions.

Part of the difficulty in assessing the role that electronic stopping has in irradiation damage is the unresolved question of what mechanism governs the coupling of electronic excitations to damage in the atomic lattice. A review of four suggested models in the context of track formation due to swift heavy ions is found in [15]. One of the commonly used models is the inelastic thermal spike model [16, 17], in which dense electronic excitations transfer energy to the lattice through electron-phonon coupling. Using this model, the contribution of electronic stopping to irradiation processes amounts on the atomic level to local heating along the ion trajectory.

One can distinguish between three kinds of cooperative effects that could be

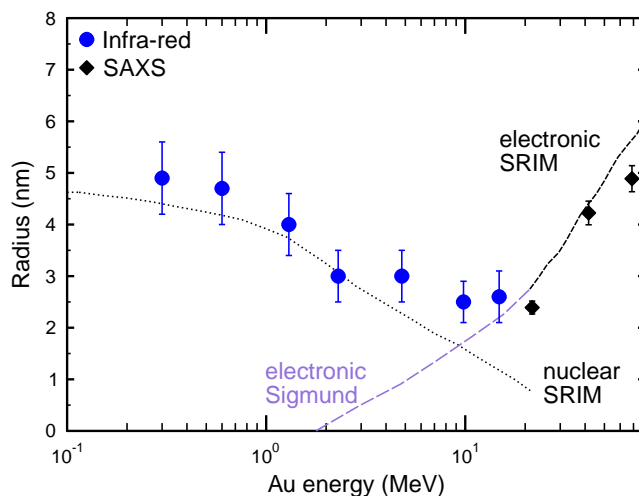


Figure 1. Increased damage radius in the intermediate energy regime due to electronic energy deposition effect. After Toulemonde *et al* [13].

observed when ions interact with both nuclei and electrons. When nuclear and electronic energy deposition produce damage at the same time in the same region of space and the total damage is the sum of the damage that they would produce separately, this can be considered an *additive* synergy. If the damage is larger than the sum of the nuclear and electronic effect, this can be considered a *nonlinear* synergy. Finally, it is also reasonable to argue that the heating introduced by electronic effects could anneal some of the nuclear damage [18], hence, resulting in less damage. The electronic energy loss then provides a competing *annealing* effect, as observed by Nagata *et al* [14] for H and He irradiation of silica.

Assuming that the effect of ionization processes from heavy ions in silica can be approximated as local heating, we present here a new approach to determining the separate and combined effect of nuclear and electronic stopping in producing irradiation damage using atomistic simulation methods. Simulations are not limited to what is experimentally possible; we can switch on and off either damage process to study them separately and together. In this work, we therefore simulate the experimental conditions in Toulemonde’s work [13] (Figure 1) using molecular dynamics (MD) methods in order to isolate the contributions of the two mechanisms and provide further insight into the interaction between nuclear and electronic energy deposition by ions.

2. Methods

An amorphous SiO_2 simulation cell was produced using the Wooten-Winer-Weaire Monte Carlo bond switching algorithm [19] in the BOMC code [20] and later relaxed in MD with the Watanabe-Samela Si-O potential [21, 22]. Details can be found elsewhere [23]. All MD simulations were performed at 300 K in a $26 \times 26 \times 26 \text{ nm}^3$ (1.1 million atoms) cell of amorphous SiO_2 with the MD code PARCAS [24]. The Au

ion energies studied are given in Table 1 and were chosen to correspond to the energies in the experimental study by Toulemonde *et al* [13], in which the ion energy ranges from low energies, at which nuclear stopping (S_n) is dominant, to very high energies, at which electronic stopping (S_e) is dominant.

In the present work, we simulate the experimental conditions for ion irradiation of a 104 nm thick SiO_2 film. MD simulation of a full cascade in SiO_2 initiated by a MeV energy ion requires substantial computational resources. This problem was avoided by applying the binary collision approximation (BCA) technique to calculate statistically probably sets of recoils generated by the passing ion in a box of the same size as the MD cell (cube of side length 26 nm), located in the middle of the 104 nm film (Figure 2(a)).

We will first describe the BCA methods used to produce the recoil scenarios that served as input for the collision cascade part of the MD simulations. For the BCA simulations, we used the CASWIN code [25], in which both ion-target collisions and the following collisions of all knocked on atoms are modeled in a Monte Carlo algorithm. Every collision is calculated by solving the collision integral as in [26]; the distance between the atoms of two consecutive collisions is fixed to the average interatomic distance in order to correspond to the atomic density of the MD cell. The actual location of the next collision is a Monte Carlo choice of the atom coordinates within the area per atom normal to the direction of the projectile. The element of the next knocked on atom is also a Monte Carlo choice based on the relative content of each atomic species in the target.

The Ziegler-Biersack-Littmark (ZBL) universal interatomic potential [27] was used for all collisions in the BCA calculations. The initial energy of incident ions were chosen to correspond to the experimental values; however, the information on the knocked-on recoils were collected only within a box geometrically identical to the MD cell. The box was chosen to be located in the middle of the film to make the ion energy inside the MD cell approximately correspond to the average energy of ions through the film in the experiments.

BCA calculations involve the collisions of the incident ion, as well as collisions between these primary atomic recoils and other atoms. For this study, the simplest approach would be to record the velocities and positions of all these *primary* recoils that appear inside the equivalent MD cell volume and import those positions and velocities into the MD simulation cell and let the subsequent displacement events evolve in the MD environment. Two reasons prevent us from doing that. One is that primary recoils with very high velocity are impractical to simulate in the MD algorithm. Another, more important, reason is that primary recoils initiated *outside* the arbitrarily chosen MD cell volume can yield extensive subcascades *inside* the volume of the MD cell (see Figure 2). For these reasons, the subcascades of primary recoils in the BCA calculation are followed down to a cutoff energy for validity of the BCA (defined below).

The lower limit of projectile energy at which the BCA approach is still valid, i.e. at which multibody collisions can be ignored, depends on the nature of the ion and the target. A simple estimate of the lower limit, suggested by Hobler and Betz [28], shows

Table 1. Au ion energies and stopping powers in SiO₂ predicted by SRIM [26]. Electronic stopping values at low energies ([†]) are overestimated by SRIM and were calculated using reciprocity theory [29].

Energy (MeV)	S _e (keV/nm)	S _n (keV/nm)	S _{tot} (keV/nm)
0.6	0.36 [†]	3.3	3.7
1.3	0.54 [†]	2.9	3.4
2.3	0.70 [†]	2.5	3.2
4.8	1.2 [†]	1.8	3.0
9.8	2.1 [†]	1.2	3.2
22.7	3.9	0.74	4.6
46.1	7.4	0.45	7.9
76.5	11	0.31	11

that the interactions between a gold ion and silicon atoms are binary to an accuracy of 5% even at ion energies as low as 500 eV. We increased the lower limit to 1 keV to ensure sufficient accuracy. In our BCA simulations, hence, we followed each branch of the full cascade evolution until a recoil with energy equal to or below 1 keV was produced.

For each ion energy, at least 10,000 ion impact scenarios were generated to ensure sufficient statistics. The positions and velocities of all recoils, at or below 1 keV, contained within the equivalent MD cell volume in the middle of the film thickness were recorded in a file later used as input in the MD simulations. Out of the 10,000 ion impact scenarios generated by the BCA calculations, five impact scenarios at each energy were chosen randomly for the MD simulations. For each chosen scenario, the positions and velocities of the recoils were imported into the MD cell, and the displacement damage was allowed to evolve to completion in the MD simulations.

The radial distribution of electronic heating (the details of which we explain later) was deposited assuming an ion trajectory that is not deflected from its original direction. In the BCA calculations, however, the ion trajectory is deflected due to collisions. To ensure spatial overlap between the electronic heating and collision cascade, the positions of each ion and of the produced recoils were shifted to make the ion pass through the center of the MD simulation cell. The maximum deviation of the ion track from the straight line was within 15° for the energies used in the present calculations, and in most cases much less. Figure 2(b) illustrates a typical track of the recoils collected after a Au ion with energy 2.3 MeV passed through the box of interest. The energies of the recoils are between 5 and 300 eV, which also is a typical energy range for the given ion energy.

Let us now focus on the electronic excitation part of the simulations. The effects of electronic stopping on irradiation damage were included in the classical MD simulations in the form of local heating added artificially to the lattice atoms. The amount of heat added to the lattice was estimated using the thermal spike model. In the inelastic thermal spike model [16, 17, 30], ion tracks are formed when an ion gives enough energy to target electrons to melt an area around the ion path, as the energy is transferred to the atomic lattice through electron-phonon coupling. The same heating mechanism is

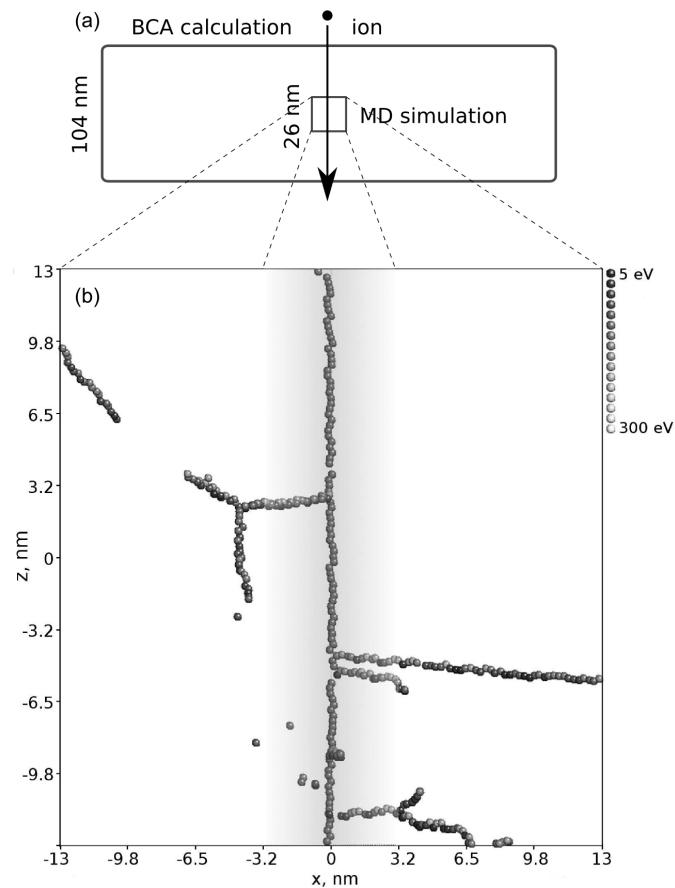


Figure 2. (a) Relation between BCA and MD simulations. (b) A typical track of generated recoils (Si and O atoms) along the Au ion path in the MD cell. The energy of the ion is 2.3 MeV, the direction of the ion is in the negative z direction. Atoms are coloured according to their recoil energy in eV, as indicated in the legend on the right. The shadowed cylindrical area covers the atoms that are given kinetic energy according to the calculated electronic energy deposition profile.

also present below the track threshold, even if the rise in temperature is not high enough to cause experimentally measurable damage.

Calculations with the two-temperature model for thermal spikes yield the kinetic energy to lattice atoms as a function of lateral distance from the ion path and time. For sake of simplicity, we chose a radial profile at time t (~ 100 fs) (when almost all of the excess energy has been transferred to the lattice) for use in the MD simulations. Electronic energy deposition profiles calculated by the inelastic thermal spike model have been used successfully in the past to model the structure of ion tracks in atomistic simulations [31, 32]. We used the same approach as in [31, 32], where kinetic energy in a random direction is added to each atom around the ion trajectory, according to a radial energy deposition profile (cf. Figure 4).

The amorphous network structure of silica is well reproduced by the Watanabe potential; however, we found the melting temperature to be significantly overestimated

(on the order of 50% higher than the literature value). To simulate the true effect of the local heating, the electronic energy deposition profiles therefore had to be scaled until the simulated track radii for the two highest energies matched corresponding experimental track radii [31]. We used density as a function of lateral distance from the ion path to define track radii in the relaxed cells. It was observed both experimentally and computationally that tracks in silica have an underdense core and an overdense shell [31, 32], and we used the outer edge of the overdense shell to define the track radius. To correct for the too high melting temperature, we only scaled the height of the distribution; the width is closely related to the predicted track radius. The derived scaling factor was then assumed to give an approximate correction for the higher melting temperature and was used for all energies.

The electronic and nuclear energy depositions were deposited simultaneously in a slightly delayed sequence. The collision cascade was initiated first, with a 0.5 fs delay between each recoil taken from the BCA set of recoils, corresponding to the chosen scenario. The thermal spike was included 20 fs after the start of the collision cascade. The short delay is consistent with the thermal spike model calculations and the time needed for energy to be dissipated and transferred to the lattice. The exact timing of events will certainly influence the course of a given collision sequence, however, we assume that the general trends are unaffected.

Each simulation was run for 100 ps to let the sharp energy gradient due to the electronic energy deposition level out. Given the ion velocity in the z direction, temperature control was used on a 5 Å thick region of the x and y boundaries to allow heat to dissipate radially from the heated cylinder as if into an infinite sink at room temperature. To avoid cascade overlap across the periodic boundaries, energetic recoils passing cell boundaries were essentially removed from the simulation cell. The number of such recoils was checked to be small enough to not affect the simulation cell composition significantly.

For the lower energies, most irradiation damage was created as damage pockets, while for the higher energies a clear core-shell structure emerged due to melting and volume expansion along the ion trajectory. We determined the amount of created damage by analyzing bond lengths and using a cut-off method to find coordination defects in the structure, since it has been found that bond scission is a common defect formation process in amorphous SiO₂ [7]. The cut-off length was set to the minimum between first and second nearest neighbours in the pair correlation function.

To find the effect of electronic heating on creating ion irradiation damage, we thus analyze the structural disorder from the two damage mechanisms separately, as well as for both the collision cascade and electronic energy deposition together. Four separate cases were studied for each of the five randomly chosen collision cascade scenarios (i.e. 20 simulations at each of the eight ion energies):

1. Only electronic energy deposition (S_e) — thermal spike
2. Only nuclear energy deposition (S_n) — displacement cascade

3. Simultaneous nuclear electronic energy deposition (20 fs delay of thermal spike) ($S_n + S_e$)
4. Nuclear and electronic energy deposition separated in time by 100 ps ($S_n + \Delta t + S_e$)

Comparison was made of the damage resulting from case 3 and case 4 to reveal whether the combined effect is an additive synergy, which is present regardless of separation in time and space, or a nonlinear synergy, which requires overlap in time and space.

3. Results and discussion

After each simulated ion interaction and relaxation, the number of coordination defects created in the cell was analyzed (Figure 3). The plot of irradiation damage defined in this way shows that the created damage scales with the total energy deposited by the ion, as measured by the total stopping power (S_{tot}) for that energy (Table 1). Both the collision cascade and electronic heating contribute to irradiation damage, hence, when they are both present in the same simulation ($S_e + S_n$) we see an enhancement of the damage level compared to the damage due to either stopping process.

Our results demonstrate that there is a clear cooperative effect of the two radiation processes with increase of ion energy. At 2.3 MeV and higher ion energies, the decrease in nuclear collision damage becomes compensated by the damage produced due to the electronic excitations in the target. Comparison between case 3 and case 4 suggest that, on the scale shown here, the damage is the same regardless of whether the heating and cascade act simultaneously or not. A direct sum of the defects in case 1 and case 2 also yields a similar result (not shown here). The results are well in line with experimental observations [13] and can be referred to as an *additive* synergy between the two kinds of energy deposition. However, examining the sets of recoils produced the BCA calculations (Fig. 2, we see that secondary recoils with sufficiently high energy to create significant subcascades can be produced further away from the ion path. For this reason, the spatial overlap of the nuclear and electronic energy deposition is small. This spatial separation also explains the independence of the final damage on the time delay of the electronic energy deposition.

Moreover, it is very noteworthy that the experimentally observed threshold for *damage creation* by Au ions in silica particles is about 0.6 keV/nm [33] and that for chemical etching of *continuous tracks* created by Au ions is 2 keV/nm [34], corresponding to ion energies above 1.3 MeV and 4.8 MeV, respectively (Table 1). (To eliminate any effect of beam energy, or the so-called velocity effect [30], we compare only to other cases of Au ion irradiation of silica.) This is consistent with the behaviour for S_e shown in Figure 3, where at low energies there is some damage due to electronic heating, and at energies higher than 5 MeV the electronic damaging mechanism becomes dominant. Hence, although below this energy the electronic damage alone would experimentally be overshadowed by the nuclear damage and hence not observable, our simulations show

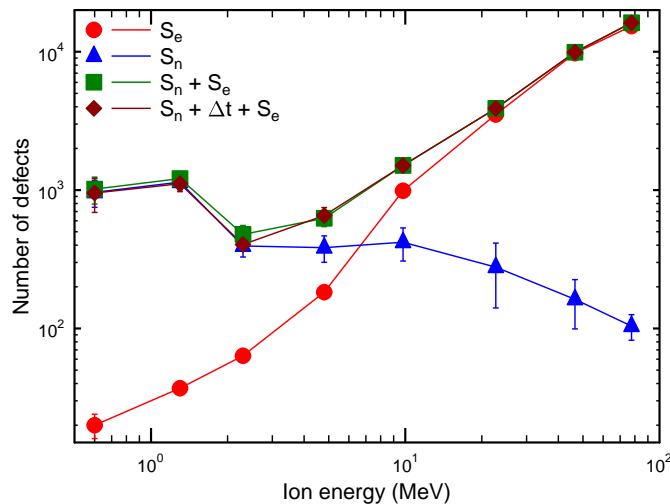


Figure 3. Number of defects in simulation cell after simulated ion bombardment. The four simulated cases are (1) only electronic energy deposition (S_e), (2) only nuclear energy deposition (S_n), (3) both mechanisms present in the same simulation ($S_n + S_e$), and (4) nuclear and electronic energy deposition separated in time ($S_n + \Delta t + S_e$).

that electronic processes can also contribute to damage creation by collision cascades below the track threshold.

To further explore a possible synergistic effect, we analyzed the density of defects as a function of lateral distance from the ion track. Since the electronic heating decreases in intensity with distance from the ion trajectory, any effect should be largest near the center of the electronic energy deposition cylinder. A comparison of the density of defects produced in the simulations with both mechanisms active simultaneously ($S_n + S_e$), and separated in time ($S_n + \Delta t + S_e$) (Figure 4), indicates a nonlinear synergistic effect on irradiation damage close to the ion path for the ion energies up to 4.8 MeV. Moreover, closer examination of cases 2 and 4 at low energies (0.6 and 1.3 MeV) suggests that electronic energy deposition that is delayed in time by 100 ps leads to statistically relevant recovery of some displacement damage within 2 to 3 nm of the ion trajectory, while simultaneous electronic and nuclear energy deposition acts synergistically (case 3). While the statistics are limited and further investigation is needed, the results demonstrate a synergy of simultaneous electronic and nuclear energy loss on damage production, while electronic energy loss delayed in time can lead to some damage recovery.

It should be noted that the relative number of defects created by the two energy deposition mechanism is not representative of the full-scale situation in the amorphous SiO_2 sample. The small size of the simulation cell leaves out a large part of the damage pockets that would result from high energy recoils, but only at large lateral distances from the ion path. This underestimation of total displacement cascade damage does not affect the damage enhancement. On the other hand, in [7], it is suggested that the

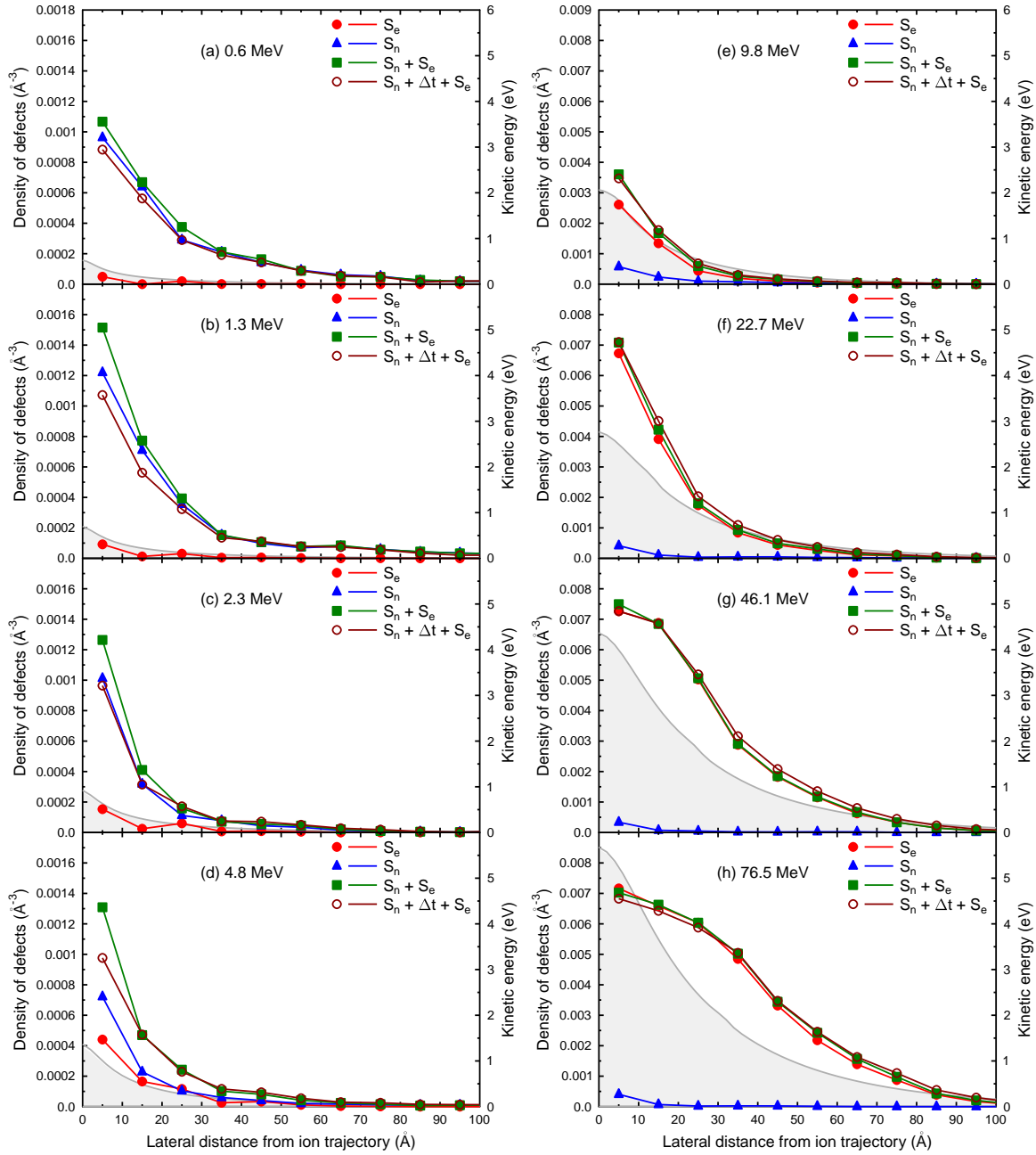


Figure 4. Density of defects as a function of lateral distance from ion trajectory for (a) 0.6 MeV, (b) 1.3 MeV, (c) 2.3 MeV, (d) 4.8 MeV, (e) 9.8 MeV, (f) 22.7 MeV, (g) 46.1 MeV, and (h) 76.5 MeV Au ions in amorphous SiO_2 . Note the different scales on the lefthand y-axis in the first and second column. The gray shaded area (righthand y-axis) represents the electronic energy deposition.

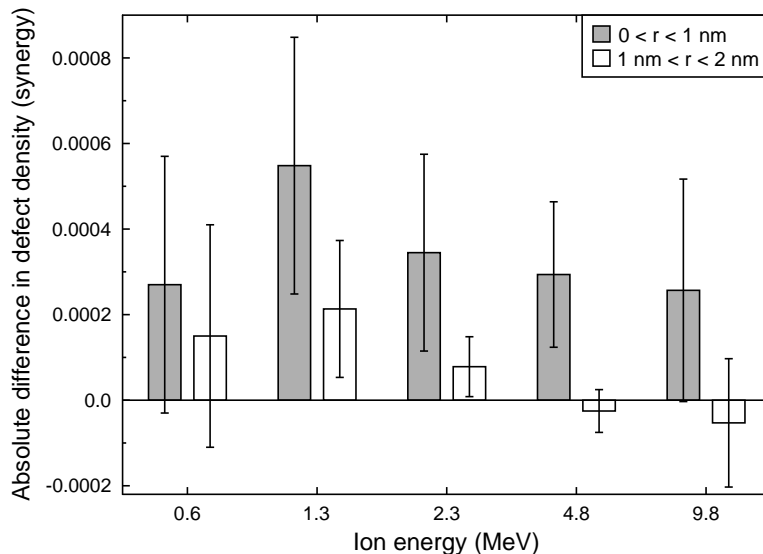


Figure 5. Difference in density of defects in the vicinity of the ion trajectory between simultaneous and sequential nuclear and electronic energy deposition (cases 3 and 4). This difference is an indication of a nonlinear synergy effect.

interaction between electronic and nuclear stopping is dose rate dependent and larger for higher dose rates. Here, we have only investigated the interaction in one single ion event, therefore, neglecting any effect of overlapping displacement cascades and thermal spikes from different ions.

4. Conclusions

The simulations of Au ion irradiation in silica demonstrate that in the intermediate range of energies, where both nuclear and electronic stopping powers are significant, there is a clear cooperation between two kinds of damage production, which is consistent with experimental results [13]. This results in an increased number of defects observed when electronic heating is included in the MD simulations, as compared to simulations where displacement cascades are the only damage mechanism. Furthermore, we observe a nonlinear synergy effect, which is most significant in the area closest to the ion trajectory where local heating due to electronic excitations is most intense and the two damage mechanisms overlap. These results clearly demonstrate that the electronic energy loss can play a role in radiation damage, and should be further studied to provide a better understanding of this effect and its significance in other materials.

Acknowledgments

W. J. Weber and Y. Zhang were supported by the U.S. Department of Energy, Basic Energy Sciences, Materials Science and Engineering Division. Part of this work was also performed within the Finnish Centre of Excellence in Computational Molecular Science (CMS), financed by The Academy of Finland and the University of Helsinki. The theoretical calculations were performed using the supercomputer resources at the National Energy Research Scientific Computing Center located at Lawrence Berkeley National Laboratory, USA, and the National IT Centre for Science CSC in Espoo, Finland.

References

- [1] Averback R S and Diaz de la Rubia T 1998 Displacement damage in irradiated metals and semiconductors *Solid State Physics* vol 51 ed Ehrenfest H and Spaepen F (New York: Academic Press) pp 281–402
- [2] Kanjijal D 2001 *Current Science* **80** 1560
- [3] Toulemonde M, Ramos S M M, Bernas H, Clerc C, Canut B, Chaumont J and Trautmann C 2001 *Nucl. Instrum. Meth. Res. Phys. B* **178** 331
- [4] Toulemonde M, Assman W, Trautmann C, Gruner F, Mieskes H D, Kucal H and Wang Z G 2003 *Nucl. Instr. Meth. Phys. Res. B* **212** 346–357
- [5] Weber W J, Ewing R C, Angell C A, Arnold G W, Cormack A N, Delaye J M, Grisom D L, Hobbs L W, Navrotsky A, Price D L, Stoneham A M and Weinberg M C 1997 *J. Mater. Res.* **12** 1946
- [6] Presby H M and Brown W L 1974 *Appl. Phys. Lett.* **24** 511
- [7] EerNisse E P and Norris C B 1974 *J. Appl. Phys.* **45** 5196
- [8] Jaque F and Townsend P D 1981 *Nucl. Instrum. Meth.* **182/183** 781
- [9] Busch M C, Slaoui A, Siffert P, Dooryhee E and Toulemonde M 1992 *J. Appl. Phys.* **71** 2596
- [10] Polman A and Poate J M 1993 *J. Appl. Phys.* **73** 1669
- [11] Devine R A B 1994 *Nucl. Instrum. Meth. Phys. Res. B* **91** 378–390
- [12] Itoh N and Stoneham A M 2001 *Materials Modification by Electronic Excitation* (Cambridge University Press)
- [13] Toulemonde M, Weber W J, Li G, Shutthanandan V, Kluth P, Yang T, Wang Y and Zhang Y 2011 *Phys. Rev. B* **83** 054106
- [14] Nagata S, Katsui H, Tsuchiya B, Inouye A, Yamamoto S, Toh K and shikma T 2009 *J. Nucl. Mater.* **386-388** 1045
- [15] Itoh N, Duffy D M, Khakshouri S and Stoneham A M 2009 *J. Phys.: Condens. Matter* **21** 474205
- [16] Toulemonde M, Dufour C and Paumier E 1992 *Phys. Rev. B* **46** 362
- [17] Toulemonde M, Dufour C, Meftah A and Paunier E 2000 *Nucl. Instr. Meth. Phys. Res. B* **166-167** 903–912
- [18] Wang Z G, Dufour C, Paumier E and Toulemonde M 1996 *Nucl. Instrum. Meth. Phys. Res. B* **115** 577
- [19] Wooten F, Winer K and Weaire D 1985 *Phys. Rev. Lett.* **54** 1392
- [20] von Alftan S, Kuronen A and Kaski K 2003 *Phys Rev. B* **68** 073203
- [21] Watanabe T, Yamasaki D, Tatsumura K and Ohdomari I 2004 *Appl. Surf. Sci.* **234** 207–213
- [22] Samela J, Nordlund K, Popok V N and Campbell E E B 2008 *Phys. Rev. B* **77** 075309
- [23] Djurabekova F and Nordlund K 2008 *Phys. Rev. B* **77** 115325
- [24] Nordlund K 2006 PARCAS computer code. The main principles of the molecular dynamics algorithms are presented in [35, 36]. The adaptive time step and electronic stopping algorithms are the same as in [37]

- [25] Pugacheva T S, Djurabekova F G and Valiev S K 1998 *Nucl. Instr. Meth. Phys. Res. B* **141** 99–104
- [26] Ziegler J F SRIM-2008 software package, available online at <http://www.srim.org>.
- [27] Ziegler J F, Biersack J P and Littmark U 1985 *The Stopping and Range of Ions in Matter* (New York: Pergamon)
- [28] Hobler G and Betz G 2001 *Nucl. Instr. Meth. Phys. Res. B* **180** 203
- [29] Sigmund P 2008 *Eur. Phys. J. D* **47** 45–54
- [30] Meftah A, Costantini J M, Khalifaoui N, Boudjadar S, Stoquert J P, Studer F and Toulemonde M 2005 *Nucl. Instrum. Meth. Phys. Res. B* **237** 563
- [31] Kluth P, Schnohr C S, Pakarinen O H, Djurabekova F, Sprouster D J, Giulian R, Ridgway M C, Byrne A P, Trautmann C, Cookson D J, Nordlund K and Toulemonde M 2008 *Phys. Rev. Lett.* **101** 175503
- [32] Pakarinen O H, Djurabekova F, Nordlund K, Kluth P and Ridgway M C 2009 *Nucl. Instr. Meth. Phys. Res. B* **267** 1456
- [33] van Dillen T, Snoeks E, Fukarek W, van Kats C M, Velikov K P, van Blaaderen A and Polman A 2001 *Nucl. Instrum. Meth. Phys. Res. B* **175-177** 350
- [34] Jensen J, Razpet A, Skupiński M and Possnert G 2006 *Nucl. Instrum. Meth. Phys. Res. B* **243** 119
- [35] Nordlund K, Ghaly M, Averback R S, Caturla M, Diaz de la Rubia T and Tarus J 1998 *Phys. Rev. B* **57** 7556–7570
- [36] Ghaly M, Nordlund K and Averback R S 1999 *Phil. Mag. A* **79** 795
- [37] Nordlund K 1995 *Comput. Mater. Sci.* **3** 448